

# Rotated Robustness: A Training-Free Defense against Bit-Flip Attacks on Large Language Models

Deng Liu, *Student Member, IEEE*, and Song Chen, *Member, IEEE*

**Abstract**—Hardware faults, specifically bit-flips in quantized weights, pose a severe reliability threat to Large Language Models (LLMs), often triggering catastrophic model collapses. We demonstrate that this vulnerability fundamentally stems from the spatial alignment between sensitive weight bits and extreme activation outliers, which causes a single hardware fault to be massively amplified. To address this, we propose Rotated Robustness (RoR), a training-free defense utilizing orthogonal Householder transformations. By applying an orthogonal rotation to the activation space, RoR geometrically smooths extreme outliers across all feature dimensions. This mechanism effectively breaks the alignment between outliers and vulnerable weights, mathematically guaranteeing original model accuracy. Extensive empirical evaluations across Llama-2/3, OPT, and Qwen families demonstrate the superior reliability of our approach. Under random bit-flip attacks, RoR reduces the stochastic collapse rate from 3.15% to 0.00% on Qwen2.5-7B. Furthermore, under severe targeted attacks with 50 Progressive Bit Search flips, RoR sustains robust reasoning on Llama-2-7B, maintaining a 43.9% MMLU accuracy that nearly matches its 45.2% unattacked accuracy, while competing defenses collapse to random guessing. Most notably, against the Single-Point Fault Attack (SPFA)—the most aggressive targeted threat—RoR exponentially inflates the attack complexity from a few bits to over 17,000 precise bit-flips. With a negligible storage overhead of 0.31% and a minimal inference latency increase of 9.1% on Llama-2-7B, RoR achieves true lossless robustness, providing a practical and highly reliable defense for LLM deployment.

**Index Terms**—Large Language Models, Bit-Flip Attacks, Hardware Fault Tolerance, Model Robustness, Orthogonal Transformation.

## I. INTRODUCTION

Large Language Models (LLMs) have significantly advanced the field of artificial intelligence [1]. With billions of parameters, models like Llama 2/3 [2], [3], Qwen [4], and GPT-4 [5] now excel at complex reasoning tasks [6]. As a result, their deployment is rapidly expanding from high-performance GPU clusters [7] to edge devices [8], powering critical applications such as autonomous agents [9] and financial analysis [10]. However, deploying these models on physical hardware exposes them to memory-level reliability threats. The Rowhammer vulnerability [11], a hardware flaw in DRAM, allows attackers to flip memory bits by repeatedly activating specific rows, causing electrical charge leakage

into adjacent cells. Recent systematic evaluations, such as the end-to-end BitMine framework [12], have demonstrated that software-induced DRAM faults can be efficiently and deterministically triggered across modern architectures by reverse-engineering proprietary memory address mappings. This fundamental vulnerability has enabled precise Bit-Flip Attacks (BFAs) [13], [14] that directly alter the stored weights of a neural network.

Unlike input-level adversarial examples, BFAs modify the model parameters directly, exposing a critical structural fragility within LLMs. While conventional wisdom suggests that billion-parameter models possess inherent statistical redundancy, recent empirical evidence invalidates this assumption by exposing extreme parameter sensitivity. Targeted bit-flips can completely bypass this presumed redundancy to inflict devastating consequences. For instance, ONEFLIP [15] demonstrates that a single bit-flip is sufficient to inject stealthy backdoors into deployed models. Similarly, AttentionBreaker [16] demonstrates that altering just three bits in an 8-bit quantized LLaMA3-8B model triggers a catastrophic functional collapse, plummeting its accuracy on the MMLU benchmark from 67.3% to exactly 0%. These findings confirm that hitting vulnerable bits causes the model’s perplexity (PPL) to explode by orders of magnitude, highlighting the severe operational risks of hardware-induced weight bit-flips.

Defending against BFAs in billion-parameter LLMs remains profoundly challenging. Existing defenses mainly fall into two paradigms, both of which struggle with the strict efficiency and utility demands of LLMs. *Detection-based methods* [17]–[21] employ runtime monitors or software-based ECC. However, verifying integrity at every layer creates severe synchronization barriers and consumes critical memory bandwidth, exacerbating the memory-bound bottlenecks of token generation. Conversely, *weight-robustness methods* compromise either efficiency or model utility. Robust retraining or fine-tuning [22], [23] is computationally prohibitive at the LLM scale and risks catastrophic forgetting. Meanwhile, encoding schemes [24], [25] mandate extra decoding steps on the critical inference path, introducing unacceptable computational and memory traffic overheads.

*Our Insight: Outlier Alignment and Amplification.* We argue that the catastrophic fragility of LLMs under bit-flips is fundamentally driven by the spatial alignment between corrupted weights and extreme activation outliers. In Transformers, specific feature channels frequently emerge as extreme outliers, reaching magnitudes up to  $20\times$  the average [26], [27]. Consequently, when a stochastic memory fault corrupts a weight parameter that interacts directly with these outlier channels, the initial error undergoes severe multiplicative

This work was supported in part by the Strategic Priority Research Program of the CAS under Grant XDB0660000, and in part by the National Natural Science Foundation of China under Grant 92473114. (Corresponding author: Song Chen.)

Deng Liu and Song Chen are with the School of Microelectronics, University of Science and Technology of China, Hefei 230026, China (e-mail: ld153@mail.ustc.edu.cn; songch@ustc.edu.cn).

Preprint. Under review at IEEE Transactions on Information Forensics and Security.

amplification. This massive perturbation cascades through and corrupts subsequent layers, triggering an irreversible network collapse and thus manifesting as the observed Single Point of Failure (SPoF) phenomenon.

*Our Approach: RoR.* We propose **Rotated Robustness (RoR)**, a training-free defense method based on orthogonal Householder transforms [28]. RoR applies a targeted rotation to the activation space, geometrically smoothing the spike energy of outliers across all feature dimensions and breaking the fatal alignment between these outliers and vulnerable weights. This effectively reduces error amplification under both random and targeted bit-flips, while mathematically guaranteeing that the original accuracy of the model remains unaffected due to the orthogonality of the transformation.

Our main contributions are summarized as follows:

- *Vulnerability Analysis & Training-Free Defense:* We identify the multiplicative amplification caused by the spatial alignment of weight errors and activation outliers as the cause of SPoFs in LLMs. To address this, we introduce RoR, a geometrically rigorous, training-free defense that leverages Householder transformations to smooth these outliers. This orthogonal rotation mathematically guarantees the preservation of the model’s original accuracy without requiring architectural modifications.
- *Superior Robustness & Task Generalization:* Extensive evaluations across diverse LLM families demonstrate RoR’s decisive superiority. It perfectly mitigates random hardware faults, reducing the stochastic collapse rate from 3.15% to **0.00%** on Qwen2.5-7B. Under severe targeted attacks (50 PBS flips), RoR sustains robust reasoning on Llama-2-7B with 43.9% MMLU accuracy, nearly matching its unattacked baseline (45.2%). Most notably, against the devastating Single-Point Fault Attack (SPFA), RoR exponentially inflates the attack cost: inducing a model collapse requires over 17,000 precise bit-flips, exposing the extreme fragility of unprotected baselines and recent defenses that collapse within a mere handful of flips ( $\leq 7$ ).
- *Extreme Inference Efficiency:* By strictly preserving hardware-friendly dense low-rank matrix multiplications and storing only compact WY representations, RoR incurs negligible storage overhead ( $< 0.4\%$ ) and minimal latency impact ( $+9.1\% \sim +19.2\%$ ), providing a highly practical foundation for securing LLM deployments.

## II. BACKGROUND AND THREAT MODEL

### A. LLM Inference and Quantization

Modern Large Language Models (LLMs) are fundamentally built upon the Transformer architecture [29]. A standard Transformer block comprises two primary sub-layers: Multi-Head Self-Attention (MHSA) and a Feed-Forward Network (FFN). The computational backbone of these blocks relies on dense linear transformations—General Matrix Multiplications (GEMMs). Formally, given an input token sequence (or activation matrix)  $\mathbf{X} \in \mathbb{R}^{T \times d}$ , a linear layer computes:

$$\mathbf{Y} = \mathbf{X}\mathbf{W} \quad (1)$$

where  $\mathbf{W} \in \mathbb{R}^{d \times d'}$  is the weight matrix. As illustrated in Figure 1, the MHSA layer projects inputs into Queries, Keys, and Values via learnable weight matrices ( $\mathbf{W}_Q, \mathbf{W}_K, \mathbf{W}_V$ ). Similarly, the FFN consists of large linear transformations interleaved with a non-linear activation function.

To alleviate memory and computational overhead during inference, Post-Training Quantization (PTQ) has emerged as a standard deployment paradigm [30]. In uniform quantization, high-precision weight elements  $w \in \mathbf{W}$  are mapped to low-bit integers (e.g., INT8) using scaling factor  $s$  and zero-point  $z$ :

$$w_q = \text{Clamp} \left( \left\lfloor \frac{w}{s} \right\rfloor + z, -2^{b-1}, 2^{b-1} - 1 \right) \quad (2)$$

These quantized parameters  $w_q$  permanently encode the semantic knowledge and reasoning capabilities acquired during the pre-training phase.

### B. Threat Model: Hardware Faults and Adversary Capabilities

Since quantized parameters physically encode model intelligence, bit-level alterations directly corrupt an LLM’s reasoning capabilities. In real-world deployments, these memory-level corruptions manifest through two primary **physical corruption mechanisms**. First, adversaries can maliciously induce deterministic bit-flips via the **Rowhammer** vulnerability [11]. By exploiting electrical charge leakage between adjacent DRAM cells, attackers can precisely target neural network weights [12] to enable gradient-guided exploitation. Second, DRAM cells are susceptible to stochastic, unguided bit-flips triggered by transient physical disturbances, such as cosmic ray radiation [31] or aggressive undervolting in edge environments [32]. Based on these mechanisms and the adversary’s access to model internals, we categorize the threat landscape into three hierarchical models:

1) *Black-Box (Stochastic):* The adversary has no knowledge of the model’s architecture or parameters. Corruptions are unguided and stochastic, representing uninformed bit-flips at a specific Bit Error Rate (BER). This model realistically accounts for natural hardware soft errors, such as Single Event Upsets (SEUs) from cosmic radiation [31] or instability from extreme dynamic voltage scaling [32].

2) *Gray-Box (Targeted):* The attacker knows the model architecture and weight values but is blind to the internal defense configuration. This allows for gradient-guided or heuristic-based exploits, such as Progressive Bit Search (PBS) [13] and AttentionBreaker [16], to iteratively identify and flip the most vulnerable bits for maximal output degradation.

3) *White-Box (Defense-Aware):* Representing the most severe scenario, the attacker has unrestricted access to model weights, gradients, and the complete algorithmic logic of the defense. This aligns with Kerckhoffs’s principle [33] and the proliferation of open-weight models like Llama-2 [2]. As illustrated in Fig. 1, the adversary can execute defense-aware attacks explicitly tailored to bypass protection. By pinpointing and flipping a single critical bit in DRAM, the attacker exploits the Single Point of Failure (SPoF) phenomenon, where a localized physical error multiplicatively amplifies across layers to corrupt the final output [34]. We formally analyze the underlying mechanics of SPoF in Sec. III.

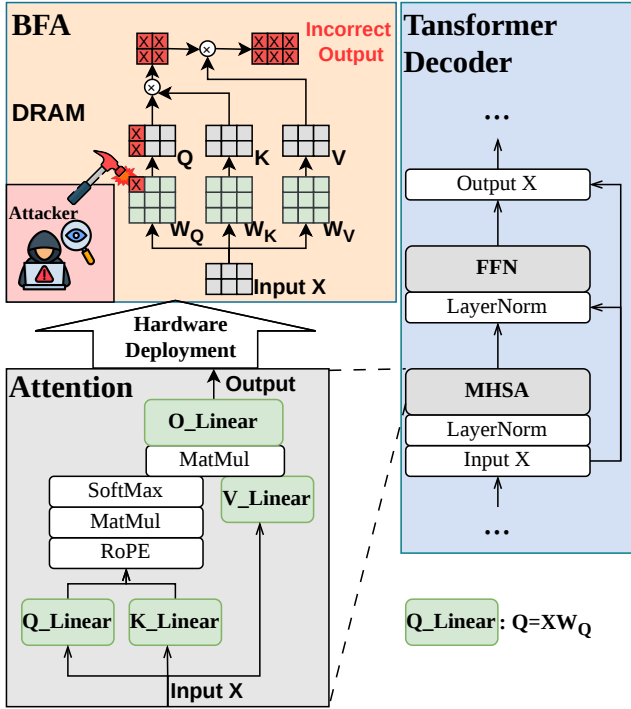


Fig. 1. **Bit-flip error propagation in Transformers.** A targeted physical attack (e.g., Rowhammer) corrupts a single bit in a weight matrix (e.g.,  $W_Q$ ) stored in DRAM. This localized error multiplicatively amplifies through subsequent Multi-Head Self-Attention (MHSA) and feed-forward layers, ultimately causing catastrophic output corruption.

### C. Defense Objectives

Practical Bit-Flip Attacks are strictly constrained by the physical limits of hardware primitives. Rowhammer-class exploits, for instance, can only induce a sparse and spatially uncontrolled set of flips within localized DRAM rows. Driven by these constraints and the high-utility requirements of LLMs, an effective defense must satisfy four core objectives:

- 1) *Reliability (Black-Box)*: The defense must effectively mitigate catastrophic failures under stochastic, unguided bit-flip errors to ensure high operational reliability.
- 2) *Complexity (Gray/White-Box)*: The defense must drastically increase the number of targeted flips required for model collapse. This ensures the necessary attack complexity fundamentally exceeds the localized physical limitations of practical Rowhammer-scale exploits.
- 3) *Utility Preservation*: The mechanism must maintain the LLM’s original reasoning capabilities and generative accuracy, ensuring zero or near-zero degradation of the pre-trained baseline performance.
- 4) *System Efficiency*: To support high-throughput deployment, the defense must minimize both inference latency and storage overhead, avoiding the synchronization or memory-bound bottlenecks inherent in prior schemes.

## III. MOTIVATION

### A. The Low-Probability SPoF Phenomenon

Prior research has predominantly focused on gradient-based targeted Bit-Flip Attacks (BFA) [13], [35], while the threat of

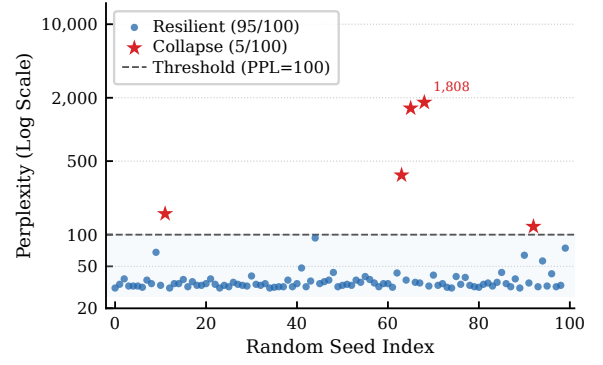


Fig. 2. **The SPoF Phenomenon.** PPL fluctuations of OPT-125M under random bit-flips (100 seeds). Most trials survive (blue dots), while specific seeds trigger catastrophic PPL explosions (red star).

stochastic bit-flips—stemming from hardware soft errors or voltage instability—is often trivialized. A prevailing assumption is that the massive parameter redundancy of LLMs acts as a natural buffer against random faults. However, our empirical analysis fundamentally challenges this belief.

We conducted extensive simulations on OPT-125M by injecting random bit-flips ( $BER = 3 \times 10^{-4}$ ) across 100 distinct seeds. As illustrated in Fig. 2, we observe a stark dichotomy in model behavior. While the model maintains *silent resilience* in most trials, approximately 5% of the cases exhibit a sudden, catastrophic *system collapse*. In these instances, the Perplexity (PPL) explodes by orders of magnitude (e.g., from  $\sim 30$  to 1808), leading to a complete loss of reasoning capability. We define this low-probability catastrophic collapse as the Single Point of Failure (SPoF) phenomenon.

This phenomenon proves that LLMs do not possess full statistical redundancy; instead, critical SPoFs exist within the vast parameter space. For safety-critical deployments, even a non-zero probability of such collapse is unacceptable, necessitating a defense that neutralizes these latent vulnerabilities.

### B. Spatial Alignment of SPoFs with Outlier Features

To investigate the cause of sporadic collapses, we employ a binary search strategy ( $\mathcal{O}(\log N)$ ) to pinpoint critical bits among billions of parameters. Tracing the most severe failures in OPT-125M (seeds 68 and 65) reveals that despite differing bit positions, both SPoFs converge on the *same weight row* (index 706), which interacts with activation channel 706.

As visualized in Fig. 3, channel 706 is an extreme outlier whose magnitude ( $\sim 6$ ) exceeds the typical range ( $[-0.2, 0.2]$ ) by over  $30\times$ . In a standard linear layer ( $\mathbf{Y} = \mathbf{XW}$ ), the output perturbation  $\Delta y_{i,k}$  at token  $i$  caused by a weight bit-flip  $\Delta W_{j,k}$  is:

$$\Delta y_{i,k} = x_{i,j} \cdot \Delta W_{j,k} \quad (3)$$

where  $x_{i,j}$  represents the activation at channel  $j$ . When a fault corrupts the Most Significant Bits (MSBs) of a weight row  $j$  that aligns with an outlier activation channel ( $|x_{i,j}| \gg 0$ ), the error undergoes severe multiplicative amplification across every token.

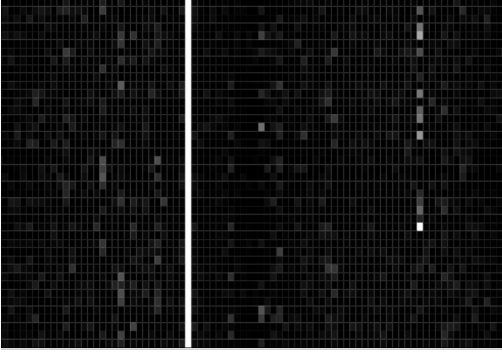


Fig. 3. **Spatial Alignment of SPoFs.** Visualization of activations in OPT-125M layer2.fc1. Channel 706 (white vertical stripe) exhibits extreme magnitudes ( $\sim 6$ ) compared to surrounding channels (dark background), creating a structural vulnerability for bit-flip in the corresponding weight row.

Our findings empirically confirm that latent SPoFs are structurally anchored to these specific outlier dimensions, providing the key motivation for the geometric delocalization in our proposed RoR.

#### IV. METHODOLOGY

In this section, we analyze the outlier vulnerability and propose RoR, a highly efficient, precision-guided defense utilizing Compact WY Householder transformations [36].

##### A. Vulnerability Analysis: Bounding the Worst-Case Error

As established in Sec. III (Eq. 3), a hardware-induced bit-flip  $\Delta W_{j,k}$  is multiplicatively amplified by the corresponding activation magnitude  $x_{i,j}$  during the forward pass. Because LLMs autoregressively condition future predictions on past outputs, corrupting the hidden state of *even a single token* can derail the entire generation process and trigger a cascading Single Point of Failure (SPoF).

To prevent such catastrophic collapses, a robust defense must strictly bound the worst-case error injection across the sequence. The maximum perturbation introduced to any token  $i$  is directly governed by the Infinity Norm ( $L_\infty$ ) of the corresponding activation channel  $j$ :

$$\max_i |\Delta y_{i,k}| = |\Delta W_{j,k}| \cdot \|\mathbf{X}_{:,j}\|_\infty \quad (4)$$

where  $\|\mathbf{X}_{:,j}\|_\infty = \max_i |x_{i,j}|$ . Defining the vulnerability metric through  $L_\infty$  rigorously captures both continuous outlier stripes (Fig. 3) and isolated extreme spikes, ensuring no single-token failure goes undetected.

**Empirical Detection Strategy.** Let  $\mathbf{m} \in \mathbb{R}^{d_{in}}$  be the vector of channel-wise  $L_\infty$  norms, with mean  $\mu$  and standard deviation  $\sigma$ . To precisely identify critical channels while avoiding false positives, we define a composite outlier threshold  $\tau$ :

$$\tau = \max \left( \underbrace{\mu + \alpha \cdot \sigma}_{\text{Statistical}}, \underbrace{2\mu}_{\text{Relative}}, \underbrace{1.0}_{\text{Absolute}} \right) \quad (5)$$

where  $\alpha$  is a sensitivity hyperparameter (default  $\alpha = 6$ ). The absolute floor of 1.0 explicitly filters out inactive channels. Any channel  $j$  satisfying  $m_j > \tau$  is flagged for targeted rotation.

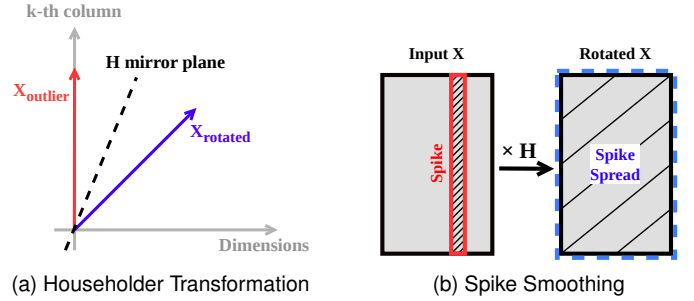


Fig. 4. **Illustration of Householder Rotation and smoothing.** (a) Geometrically,  $\mathbf{H}$  reflects the outlier vector (red) into a smoothed vector (blue). (b) In the matrix view, this operation smooths the spike of the outlier column across all dimensions.

##### B. RoR Framework: Lossless Outlier Smoothing

To explicitly neutralize the identified structural vulnerabilities, we propose Rotated Robustness (RoR). The core principle of RoR is to apply a targeted orthogonal rotation  $\mathbf{Q} \in \mathbb{R}^{d_{in} \times d_{in}}$  to the activation matrix.

We first guarantee that this defense is mathematically **lossless**. By inserting an orthogonal identity term ( $\mathbf{Q}\mathbf{Q}^\top = \mathbf{I}$ ) into the standard linear matrix multiplication, we derive:

$$\mathbf{Y} = \mathbf{X}\mathbf{W} = \mathbf{X}(\mathbf{Q}\mathbf{Q}^\top)\mathbf{W} = (\mathbf{X}\mathbf{Q})(\mathbf{Q}^\top\mathbf{W}) = \tilde{\mathbf{X}}\tilde{\mathbf{W}} \quad (6)$$

where  $\tilde{\mathbf{X}}$  and  $\tilde{\mathbf{W}}$  denote the rotated activations and pre-rotated weights, respectively. Because the final output  $\mathbf{Y}$  remains strictly identical to the clean model, RoR induces zero degradation to the LLM's baseline generative capabilities. Our objective is to construct a specific  $\mathbf{Q}$  that strictly minimizes the  $L_\infty$  peak of the rotated activations:

$$\min_{\mathbf{Q}} \|\tilde{\mathbf{X}}\|_\infty \quad \text{s.t.} \quad \mathbf{Q}^\top\mathbf{Q} = \mathbf{I} \quad (7)$$

To achieve this targeted smoothing efficiently, we employ the Householder transformation [28]. A Householder matrix  $\mathbf{H}$  is defined by a unit vector  $\mathbf{v}$ :

$$\mathbf{H} = \mathbf{I} - 2\mathbf{v}\mathbf{v}^\top \quad (8)$$

Suppose the  $k$ -th activation channel is an identified outlier, represented by the standard basis vector  $\mathbf{e}_k$ . We aim to reflect this concentrated spatial energy into a uniformly smoothed vector  $\mathbf{u} = [d_{in}^{-1/2}, \dots, d_{in}^{-1/2}]^\top$ . We construct the exact normal vector  $\mathbf{v}$  such that  $\mathbf{H}\mathbf{e}_k = \mathbf{u}$ :

$$\mathbf{v} = \mathbf{e}_k - \mathbf{u}, \quad \text{with } \mathbf{v} \leftarrow \frac{\mathbf{v}}{\|\mathbf{v}\|_2} \quad (9)$$

Applying this specific transformation perfectly redistributes the outlier spike. The resulting activation matrix becomes:

$$\mathbf{X}' = \mathbf{X}\mathbf{H} = \mathbf{X} - 2(\mathbf{X}\mathbf{v})\mathbf{v}^\top \quad (10)$$

Specifically, for the outlier column  $k$ , the transformation strictly guarantees  $\mathbf{X}'_{:,k} = \mathbf{X}\mathbf{u}$  (as illustrated in Fig. 4). This redistributes the extreme magnitude into a uniform distribution, fundamentally eliminating the  $L_\infty$  vulnerability associated with that dimension.

### C. Efficient Implementation via Compact WY Representation

In practice, a layer may contain multiple identified outliers ( $m > 1$ ). Suppressing all targets requires accumulating  $m$  sequential Householder transformations:  $\mathbf{Q} = \mathbf{H}_1 \mathbf{H}_2 \dots \mathbf{H}_m$ . While this product rigorously maintains orthogonality ( $\mathbf{Q}\mathbf{Q}^\top = \mathbf{I}$ ), sequential execution requires reading and writing the activation matrix  $m$  times, inducing severe memory access overhead and underutilizing GPU tensor cores.

To resolve this bottleneck, we leverage the Compact WY Representation [36] to mathematically fuse  $m$  sequential rotations into a single low-rank block operation:

$$\mathbf{Q} = \mathbf{I} - \mathbf{V}\mathbf{T}\mathbf{V}^\top \quad (11)$$

where  $\mathbf{V} \in \mathbb{R}^{d_{in} \times m}$  stacks the target Householder vectors, and  $\mathbf{T} \in \mathbb{R}^{m \times m}$  is an upper triangular factor matrix.

**End-to-End Deployment Pipeline.** As summarized in Fig. 5 and Alg. 1, this compact formulation allows us to decouple the RoR framework into a highly efficient offline-online pipeline:

1) *Offline Preparation & Weight Fusion:* Using calibration data, we locate the  $m$  outlier channels (Phase 1) and construct the low-rank matrices  $\mathbf{V}$  and  $\mathbf{T}$  (Phase 2). Crucially, we absorb the inverse rotation into the original model weights ( $\mathbf{W} \in \mathbb{R}^{d_{in} \times d_{out}}$ ) entirely offline (Phase 3):

$$\tilde{\mathbf{W}} = \mathbf{Q}^\top \mathbf{W} = \mathbf{W} - \mathbf{V}\mathbf{T}^\top \mathbf{V}^\top \mathbf{W} \quad (12)$$

2) *Online Activation Transform (Inference):* During deployment (Phase 4), the baseline matrix multiplication is dynamically protected by applying the low-rank WY transformation strictly to the incoming activations:

$$\tilde{\mathbf{X}} = \mathbf{X} - (\mathbf{X}\mathbf{V})\mathbf{T}\mathbf{V}^\top \quad (13)$$

This online correction is the *only* stage where RoR introduces computational overhead.

**Overhead Analysis.** Because lethal outliers are highly sparse ( $m \ll d_{in}$ , typically  $< 1\%$ ), the correction term in Eq. (13) relies entirely on skinny low-rank matrix multiplications. This operation requires approximately  $\mathcal{O}(B \cdot d_{in} \cdot m)$  FLOPs, adding strictly  $< 1\%$  latency compared to the heavy  $\mathcal{O}(B \cdot d_{in} \cdot d_{out})$  baseline matrix multiplication. Furthermore, the storage burden is restricted exclusively to the low-rank parameters  $\mathbf{V}$  and  $\mathbf{T}$ , making RoR exceptionally lightweight for memory-constrained edge deployments.

## V. EVALUATION

In this section, we conduct a comprehensive empirical evaluation of RoR, systematically examining its robustness against bit-flip attacks across black-box, gray-box, and white-box threat models, as well as its generalization to downstream tasks, computational efficiency, and sensitivity to hyperparameter configurations.

We organize our experiments to answer the following six research questions:

- **RQ1 (Black-Box Robustness):** Can RoR maintain stable model performance under random bit-flip attacks, where the attacker has no knowledge of the model internals and inflicts unguided, stochastic memory faults?

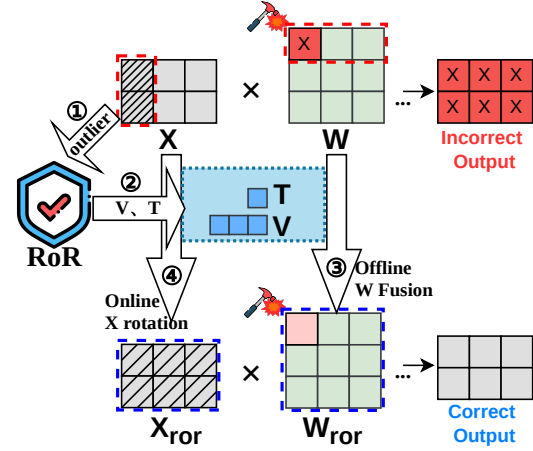


Fig. 5. **The overall framework of RoR.** The pipeline consists of four steps: Offline Outlier Identification, Compact WY Construction, Offline Weight Fusion, and Online Inference. The fusion process absorbs the majority of the computational cost offline, leaving only a negligible low-rank correction during inference.

---

### Algorithm 1 RoR: Outlier Suppression via Householder

---

**Require:** Pre-trained LLM weights  $\mathbf{W}$ , Calibration dataset  $\mathcal{D}_{cal}$ , Outlier threshold  $\alpha$

**Ensure:** Rotated weights  $\tilde{\mathbf{W}}$ , Rotation parameters  $\{\mathbf{V}, \mathbf{T}\}$

- 1: **Phase 1: Offline Outlier Identification**
  - 2: **for** each layer  $l$  in LLM **do**
  - 3:   Collect activation matrix  $\mathbf{X}^{(l)}$  using  $\mathcal{D}_{cal}$
  - 4:   Compute channel-wise peaks:  $m_k \leftarrow \|\mathbf{X}_{:,k}^{(l)}\|_\infty$
  - 5:   Compute statistics:  $\mu \leftarrow \text{mean}(\mathbf{m}), \sigma \leftarrow \text{std}(\mathbf{m})$
  - 6:   Threshold:  $\tau \leftarrow \max(\mu + \alpha \cdot \sigma, 2\mu, 1.0)$
  - 7:   Identify outlier indices:  $\mathcal{I} \leftarrow \{k \mid m_k > \tau\}$
  - 8: **end for**
  - 9: **Phase 2: Compact WY Construction**
  - 10: **for** each target layer **do**
  - 11:   Initialize  $\mathbf{V} \leftarrow [], \mathbf{T} \leftarrow []$
  - 12:   **for** each outlier index  $k \in \mathcal{I}$  **do**
  - 13:     Define target  $\mathbf{u}$  (uniform smoothed vector)
  - 14:     Compute Householder vector:  $\mathbf{v} \leftarrow \mathbf{e}_k - \mathbf{u}$
  - 15:     Update block representation  $\mathbf{V}, \mathbf{T}$
  - 16:   **end for**
  - 17: **Phase 3: Offline Weight Fusion**
  - 18:   Compute rotated weights:  $\tilde{\mathbf{W}} \leftarrow \mathbf{W} - \mathbf{V}\mathbf{T}^\top \mathbf{V}^\top \mathbf{W}$
  - 19:   Store low-rank parameters  $\mathbf{V}, \mathbf{T}$  alongside  $\tilde{\mathbf{W}}$
  - 20: **end for**
  - 21: **Phase 4: Online Inference**
  - 22: Given input activation  $\mathbf{X}$ :
  - 23: Apply low-rank rotation:  $\tilde{\mathbf{X}} \leftarrow \mathbf{X} - (\mathbf{X}\mathbf{V})\mathbf{T}\mathbf{V}^\top$
  - 24: Compute output:  $\mathbf{Y} \leftarrow \tilde{\mathbf{X}}\tilde{\mathbf{W}}$
- 

- **RQ2 (Gray-Box Robustness):** Can RoR effectively suppress catastrophic degradation under gradient-guided targeted attacks, where the attacker has partial knowledge of the model, specifically access to model weights and the ability to compute gradients?
- **RQ3 (White-Box Robustness):** Under the strongest threat model where the attacker has full access to model

internals, including weights, defense configurations, and any encryption keys, does RoR provide reliable protection against single point failure attacks?

- **RQ4 (Task Generalization):** Does the robustness conferred by RoR extend to diverse downstream tasks (e.g., HellaSwag, MMLU, PIQA), ensuring reliable performance beyond standard language modeling metrics?
- **RQ5 (Efficiency):** What are the practical inference latency and storage overheads of deploying RoR?
- **RQ6 (Ablation Study):** How do hyperparameter configurations (e.g., outlier threshold  $\alpha$ ) affect the trade-off between defensive performance and efficiency?

### A. Experimental Setup

**Implementation Details.** We implement RoR using Python 3.10 and PyTorch 2.4.1 with CUDA 12.1. All experiments are conducted on a server equipped with an Intel Xeon Platinum 8558P CPU and a single NVIDIA H200 NVL GPU, ensuring precise measurement of inference latency and supporting the intensive computations required for gradient-based attacks.

**Models.** We evaluate RoR across a diverse set of LLMs spanning multiple scales and architectures, organized by threat scenario. For black-box evaluation (RQ1), we use OPT-125M [37], Qwen2.5-0.5B, and Qwen2.5-7B [38], where smaller models facilitate large-scale statistical testing under stochastic attacks and Qwen2.5-7B assesses scalability. For gray-box evaluation (RQ2), we adopt Llama-3.2-1B [3], Llama-2-7B [2], and Qwen2.5-7B [38], covering compact to mainstream-scale architectures under gradient-guided targeted attacks. For white-box evaluation (RQ3), we use Llama-2-7B [2] and Qwen2.5-7B [38] under the strongest threat model with full model knowledge.

**Datasets.** For the primary robustness evaluation, we use WikiText-2 [39] as the canonical language modeling benchmark, quantifying degradation via Perplexity (PPL) under attack. PPL measures how confidently a model predicts held-out text, where a lower value indicates better performance and a higher value signals degraded capability. For task generalization, we additionally employ HellaSwag [40], MMLU [41], and PIQA [42], with detailed descriptions deferred to Section V-E.

**Compared Defenses.** We compare RoR against the following representative methods.

(i) *Baseline:* The vanilla quantized model with no defense applied, serving as the lower-bound reference.

(ii) *FaR [43]:* A training-free structural defense for Transformers that rewires Linear layers by redistributing the functional importance of critical neurons to non-essential ones, reducing the attack surface for gradient-based adversaries without requiring full retraining.

(iii) *RADAR [17]:* A run-time detection and recovery scheme that organizes weights into interleaved groups and computes a 2-bit checksum signature per group using masked summation. During inference, the live signature is compared against a securely stored golden signature to detect bit-flip attacks; upon detection, all weights in the compromised group are zeroed out to suppress accuracy degradation.

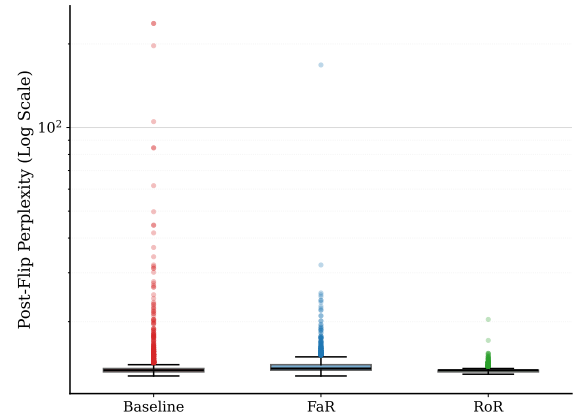


Fig. 6. Distribution of post-flip perplexity over 2,000 random bit-flip attack trials on Qwen2.5-0.5B.

### B. Black-Box Robustness under Random Bit-Flip Attacks (RQ1)

To evaluate RoR under the black-box threat model, we simulate stochastic bit-flip attacks via Monte Carlo experiments. Unlike gradient-guided attacks, random bit flips reflect the unpredictable nature of black-box adversaries who lack any knowledge of model internals, resulting in unguided and stochastic perturbations to model weights.

We conduct 2,000 independent trials on OPT-125M, Qwen2.5-0.5B, and Qwen2.5-7B under a fixed bit error rate (BER) of  $3 \times 10^{-4}$ . In each trial, bits in the model weights are randomly flipped according to the specified BER, and the resulting perplexity (PPL) on WikiText-2 is recorded.

**Results.** Table I and Fig. 6 reports the statistical robustness metrics across all three models. The *Fail Rate* denotes the probability that a single random bit flip renders the model unusable ( $\text{PPL} > 100$ ). The results reveal three key findings.

(i) *Architectural fragility varies significantly.* The legacy OPT-125M is highly vulnerable under the undefended baseline, with a 5.35% failure rate — roughly 1 in every 20 random flips triggers catastrophic collapse. The modern Qwen2.5-0.5B is comparatively more resilient (0.20%), yet its worst-case PPL still spikes to 237. Qwen2.5-7B presents a more severe result: despite a moderate 3.15% failure rate, a single unlucky flip can drive PPL to  $2.8 \times 10^5$ , confirming that larger models are not immune to catastrophic fault events.

(ii) *Existing defenses provide inconsistent protection.* FaR fails to reduce the failure rate on OPT-125M, where it marginally worsens from 5.35% to 5.40%, with the worst-case PPL remaining as high as 5920. On Qwen2.5-0.5B, FaR reduces the failure rate to 0.05% but still leaves a residual worst-case risk, as illustrated by the PPL distribution in Fig. 6 (Max PPL 168). On Qwen2.5-7B, FaR achieves a 0.00% failure rate yet leaves the mean PPL elevated at 8.10, indicating non-catastrophic but persistent degradation. Overall, FaR exhibits inconsistent effectiveness across architectures and cannot reliably suppress failure risk.

(iii) *RoR provides universal and tight protection.* RoR delivers consistent robustness across all three architectures. On OPT-125M, it reduces the failure rate by  $53\times$  (5.35% →

TABLE I  
STATISTICAL ROBUSTNESS UNDER RANDOM BIT-FLIP ATTACKS (2,000 TRIALS).

Method	OPT-125M			Qwen2.5-0.5B			Qwen2.5-7B		
	Mean PPL	Max PPL	Fail Rate (%)	Mean PPL	Max PPL	Fail Rate (%)	Mean PPL	Max PPL	Fail Rate (%)
Baseline	97.93	7616.0	5.35	14.24	237.0	0.20	374.99	$2.8 \times 10^5$	3.15
FaR [43]	113.18	5920.0	5.40	13.98	168.0	0.05	8.10	14.4	<b>0.00</b>
<b>RoR (Ours)</b>	<b>35.32</b>	<b>296.0</b>	<b>0.10</b>	<b>13.39</b>	<b>20.4</b>	<b>0.00</b>	<b>5.60</b>	<b>6.8</b>	<b>0.00</b>

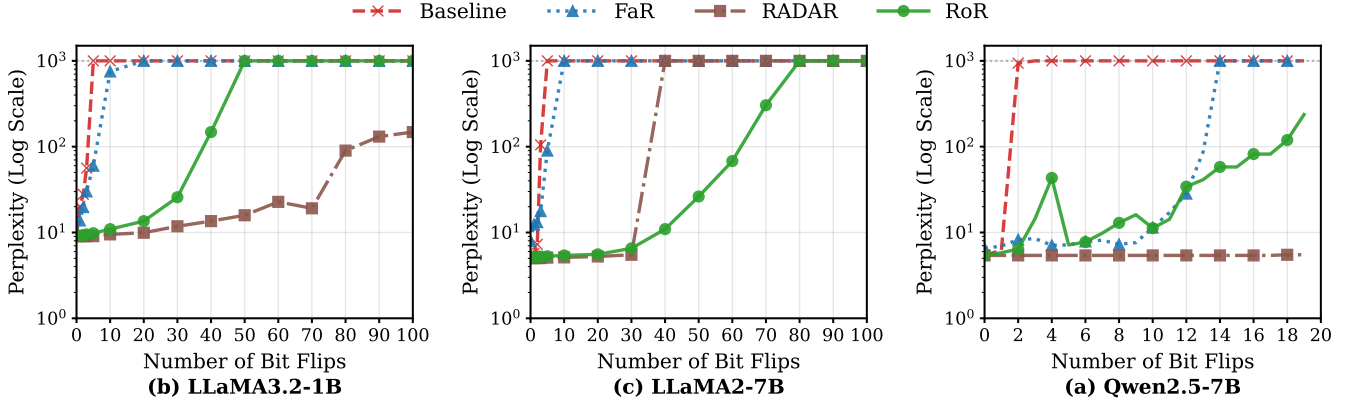


Fig. 7. PPL degradation under gray-box PBS attack (log scale). RoR consistently maintains the lowest and most stable PPL trajectory across all three architectures, while baselines collapse within a small number of flips.

0.10%) and constrains the worst-case PPL from 7616 to 296. On Qwen2.5-0.5B, RoR achieves a perfect 0.00% failure rate and suppresses the maximum PPL to 20.4. On Qwen2.5-7B, RoR similarly achieves 0.00% failure while reducing the mean PPL to 5.60 and the maximum to just 6.8 (nearly indistinguishable from original baseline inference PPL). These results confirm that RoR’s outlier smoothing mechanism effectively ensures that no single bit flip carries sufficient magnitude to trigger catastrophic degradation, thereby providing reliable stability across diverse architectures and scales.

### C. Defense Efficacy under Gray-Box PBS Attack (RQ2)

We evaluate RoR under a gray-box threat model, where the adversary employs Progressive Bit Search (PBS) [13] with knowledge of the model architecture and quantization scheme, but without access to the defense mechanism internals. We compare Baseline, FaR, RADAR, and RoR across three model scales. For clarity, all PPL curves in Fig. 7 are displayed with a maximum PPL of 1000 to facilitate visual comparison; complete numerical results are provided in Appendix A.

**Results.** Figure 7 reveals distinct vulnerability profiles across architectures.

(i) *Baseline and FaR collapse rapidly.* The unprotected Baseline is catastrophically fragile across all models. On Llama-2-7B, PPL explodes to 6720 after just 5 flips and reaches  $1.69 \times 10^9$  by flip 100. FaR introduces an original-accuracy penalty (initial PPL 8.00 vs. 5.03 on Llama-2-7B, 10.12 vs. 9.06 on Llama-3.2-1B, 6.56 vs. 5.41 on Qwen2.5-7B) and still collapses rapidly under attack — exceeding PPL 2000 within 10 flips on Llama-2-7B and PPL  $10^5$  within 16 flips on Qwen2.5-7B.

(ii) *RADAR provides strong but unstable protection.* RADAR demonstrates remarkable resilience in the early attack phase, maintaining near-original PPL across all three models up to approximately 30–40 flips. However, it suffers a sudden and severe failure beyond this point: on Llama-2-7B, PPL jumps abruptly from 5.50 at flip 30 to 2624 at flip 40, and continues rising to 8640 by flip 100. This failure stems from an inherent limitation of group checksum detection: as PBS progressively accumulates bit flips, the probability that two corrupted bits within the same group produce canceling checksum grows monotonically, eventually causing the corruption to go undetected and the recovery mechanism to never trigger.

(iii) *RoR provides smooth and sustained robustness.* In contrast, RoR preserves original accuracy without any penalty (initial PPL matches Baseline on all models) and remains stable rather than collapsing abruptly. On Llama-2-7B, PPL remains at 5.56 after 20 flips and only reaches 26.25 after 50 flips — well within usable range. On Qwen2.5-7B, RoR holds PPL below 10 for the first 6 flips and below 120 through flip 18, where Baseline has already reached  $1.95 \times 10^{11}$ . On the compact Llama-3.2-1B, RoR maintains PPL at 13.56 after 20 flips while Baseline has already collapsed beyond  $10^5$ .

RoR is the only defense that simultaneously preserves original-model accuracy and maintains reliable protection under sustained PBS attacks across diverse architectures. RADAR offers competitive early-phase protection but breaks down suddenly once attack accumulation exceeds its detection capacity, whereas FaR and Baseline offer no meaningful resistance even under a small number of bit flips.

### D. White-Box Robustness Against Single Point Failure Attacks (RQ3)

Under the white-box threat model, the adversary has complete knowledge of each defense’s internal structure, enabling *single point failure attacks* (SPFA) that exploit defense-specific vulnerabilities to amplify a minimal fault into a catastrophic model failure. The critical vulnerable bit is identified via binary search over the model weights, as introduced in Section III: for instance, on Llama-2-7B, a single flip of bit 7 at `layer1.self_attn.v_proj[1512,1100]` suffices to collapse the model, while on Qwen2.5-7B the critical location is bit 7 at `layer1.mlp.gate_proj[1923,17094]`.

**Attack Construction.** Each defense imposes a distinct exploitation requirement for the adversary to successfully replicate the SPoF phenomenon.

(i) *Baseline requires only 1 targeted bit-flip* at a weight parameter structurally aligned with an extreme activation outlier.

(ii) *FaR requires 7 coordinated flips*: given white-box access to the neuron importance redistribution mapping, the adversary identifies the target critical neuron and simultaneously corrupts the target bit along with all 6 linked non-essential neuron, completely neutralizing the rewiring protection.

(iii) *RADAR requires 2 coordinated flips*: given white-box access to the securely stored golden signature and the interleaved group partition information ( $G=512$ ), the adversary simultaneously flips the target critical bit and a carefully chosen partner bit within the same checksum group. This mutual cancellation exactly preserves the checksum, bypassing the integrity monitor while successfully inducing the original SPoF.

(iv) *RoR requires a massive sequence of coordinated flips* (e.g.,  $\sim 17,000$  flips on a single column): RoR stores the compact factors  $\mathbf{V}$  and  $\mathbf{T}$  as part of its defense configuration, which under the white-box threat model are assumed to be fully accessible to the adversary. Given these factors, the attacker can analytically reconstruct the orthogonal transformation  $\mathbf{Q} = \mathbf{I} - \mathbf{V}\mathbf{T}\mathbf{V}^\top$  and exploit the mathematical equivalence to translate a single-bit SPoF fault into a dense column attack on the rotated weights.

Specifically, the baseline forward pass satisfies:

$$\mathbf{Y} = \mathbf{X}\mathbf{W} = (\mathbf{X}\mathbf{Q})(\mathbf{Q}^\top\mathbf{W}) = \tilde{\mathbf{X}}\tilde{\mathbf{W}}, \quad (14)$$

where  $\tilde{\mathbf{W}} = \mathbf{Q}^\top\mathbf{W}$  is the stored rotated weight and  $\tilde{\mathbf{X}} = \mathbf{X}\mathbf{Q}$  is the rotated activation. A single-bit flip at the original weight  $\mathbf{W}[r, c]$  with magnitude  $\delta$  perturbs the original output by  $\Delta\mathbf{Y} = \delta \cdot \mathbf{X}_{:,r}\mathbf{e}_c^\top$  (i.e., solely affecting the  $c$ -th column of the output). To reproduce this identical output perturbation via  $\tilde{\mathbf{W}}$ , the adversary must apply a perturbation  $\Delta\tilde{\mathbf{W}}$  such that  $\tilde{\mathbf{X}}\Delta\tilde{\mathbf{W}} = \Delta\mathbf{Y}$ . This yields  $\Delta\tilde{\mathbf{W}} = \mathbf{Q}^\top\Delta\mathbf{W}$ . Since  $\Delta\mathbf{W}$  is non-zero only at  $[r, c]$ , the required perturbation becomes:

$$\Delta\tilde{\mathbf{W}}_{:,c} = \delta \cdot \mathbf{Q}_{:,r}^\top, \quad \text{where } \mathbf{Q}^\top = \mathbf{I} - \mathbf{V}\mathbf{T}^\top\mathbf{V}^\top, \quad (15)$$

which corrupts the *entire*  $c$ -th column of  $\tilde{\mathbf{W}}$  rather than a single weight element.

**Results.** Table II reports the original and post-attack PPL on WikiText-2, with the required number of coordinated flips serving as the primary metric of defense strength.

TABLE II  
WHITE-BOX SPFA RESULTS ON WIKITEXT-2.

Model	Method	Original PPL	Attack Bits	Post-Attack PPL
Llama-2-7B	Baseline	5.03	1	19,456
	FaR	8.00	7	11,072
	RADAR	5.03	2	19,456
	RoR (Ours)	5.03	<b>17,877</b>	18,304 <sup>1</sup>
Qwen2.5-7B	Baseline	5.41	1	344,064
	FaR	6.56	7	108,003,328
	RADAR	5.41	2	344,064
	RoR (Ours)	5.41	<b>17,494</b>	284,672

(i) *Existing defenses are bypassed with negligible effort.* The unprotected Baseline collapses with just 1 targeted bit-flip, reaffirming the severe threat of latent SPoFs. RADAR is neutralized by merely 2 coordinated flips, yielding an identical post-attack PPL to the Baseline (19,456 on Llama-2-7B; 344,064 on Qwen2.5-7B). This demonstrates that its integrity monitor is trivially circumvented under white-box assumptions. FaR marginally raises the exploitation requirement to 7 coordinated flips, which still reliably precipitates complete model failure.

(ii) *RoR scales the exploitation cost to physical impossibility.* In contrast, successfully replicating the SPoF phenomenon against RoR necessitates corrupting an entire column of the orthogonalized weight matrix. Measured by the IEEE-format bitwise Hamming distance between the original and perturbed weight configurations, this optimal white-box evasion translates to 17,877 simultaneous physical bit-flips on Llama-2-7B, and 17,494 on Qwen2.5-7B. State-of-the-art physical fault injection primitives, such as Rowhammer [11], can only induce sparse and spatially constrained bit-flips within a victim DRAM row. Consequently, it is physically impossible for any adversary to synchronously corrupt the thousands of precisely distributed bits required to bypass RoR. By geometrically delocalizing the vulnerability, RoR effectively shifts the SPoF exploitation cost far beyond the physical capabilities of existing hardware threat models.

### E. Task Generalization under Attack (RQ4)

A defense that solely preserves token-level fluency (perplexity) may still conceal the silent degradation of higher-level reasoning capabilities. To address this evaluation limitation, we extend our analysis beyond WikiText-2 to three diverse benchmarks, measuring whether RoR preserves semantic reasoning and world knowledge under an increasing number of targeted bit-flips.

**Benchmarks.** We evaluate on three benchmarks that probe distinct reasoning domains beyond basic language fluency. MMLU [41] is a 4-way multiple-choice benchmark; we report the macro-average accuracy over four representative domains (Elementary Mathematics, Computer Security, Philosophy, and Global Facts), where random guessing yields  $\approx 25\%$ . HellaSwag [40] is a 4-way commonsense completion

<sup>1</sup>Theoretically expected to exactly match Baseline collapse; the minor gap is attributed to quantization rounding errors introduced by weight rotation, which are amplified at severely degraded PPL.

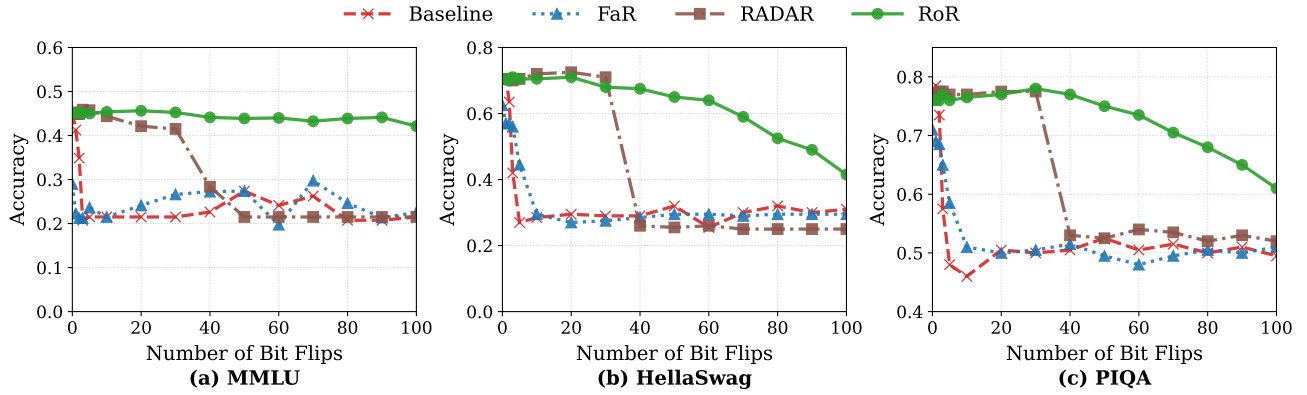


Fig. 8. **Task generalization under Progressive Bit-Search (PBS) attack on Llama-2-7B.** Accuracy on three reasoning benchmarks (MMLU, HellaSwag, PIQA) as cumulative bit flips grow from 0 to 100.

task (random baseline  $\approx 25\%$ ), reported as normalized accuracy. PIQA [42] is a 2-way physical commonsense reasoning task (random baseline  $\approx 50\%$ ). Together, these tasks evaluate STEM reasoning, specialized knowledge, abstract inference, and physical dynamics—dimensions that perplexity alone cannot comprehensively capture. Models are subjected to a Progressive Bit-Search (PBS) attack with up to 100 cumulative bit-flips on Llama-2-7B, evaluated in a 5-shot setting ( $k=5$ ,  $N=200$  instances per task).

**Results.** Figure 8 reports the accuracy across all three benchmarks as a function of the number of flipped bits. The accuracy trajectories of all competing methods closely align with the WikiText-2 PPL results in Section V-C: Baseline and FaR collapse within the first 5 flips, while RADAR sustains near-original accuracy until an abrupt, simultaneous collapse across all three metrics between flip 30 and flip 40. This mirrors the sudden catastrophic degradation previously observed in the perplexity evaluation.

*RoR is the sole method that robustly preserves task performance across all benchmarks.* At flip 50, RoR retains 43.9% MMLU, 65.0% HellaSwag, and 75.0% PIQA. Notably, even after enduring 50 targeted bit-flips, RoR’s task performance remains highly competitive with the unprotected Baseline’s original, unattacked state (Flip 0: 45.2% MMLU, 70.5% HellaSwag, 77.0% PIQA). It experiences only marginal degradation, whereas all competing defenses have completely collapsed to random guessing ( $\approx 25\%$  for MMLU/HellaSwag,  $\approx 50\%$  for PIQA). At flip 100, RoR still holds 42.1% MMLU and 61.0% PIQA, long after every competing method has degraded to near-chance performance. These results rigorously confirm that RoR’s robustness generalizes beyond perplexity, ensuring the genuine preservation of semantic and reasoning capabilities across diverse downstream tasks.

#### F. Inference Efficiency & Overhead (RQ5)

We benchmark inference latency on an NVIDIA H200 GPU (BFloat16, SeqLen=2048, Batch=16, PyTorch 2.4 with `torch.compile`) across three models: OPT-125M, Qwen2.5-0.5B, and Llama-2-7B. Results are reported in Table III.

**Defense Configurations and Storage Accounting.** Each defense stores auxiliary data beyond the quantized model weights. FaR ( $p=0.001$ ,  $K=6$  rewiring rounds) records rewired weight indices and replacement values, incurring +2.1–3.0% extra storage depending on model size. RADAR ( $G=512$ ) must materialize a full per-element  $\pm 1$  mask vector as a persistent GPU buffer in software, causing its storage to scale linearly with model size and reach +50% of the BFloat16 weight footprint—far beyond the <6 KB reported in the original paper, which assumes a dedicated hardware pipeline. RoR ( $\alpha=6.0$ ) stores only the compact Householder factors  $V \in \mathbb{R}^{d \times m}$  and  $T \in \mathbb{R}^{m \times m}$  per protected layer, yielding merely +0.17–0.31% extra storage across all models—one to three orders of magnitude smaller than the competing defenses.

**Empirical Latency.** RoR incurs a modest latency overhead of +11.9% on OPT-125M, +19.2% on Qwen2.5-0.5B, and +9.1% on Llama-2-7B, consistently the lowest among all defenses. The gap between the theoretical <1% FLOPs increase and the observed  $\sim 10$ –20% latency on smaller models reflects that the WY update introduces memory-bandwidth pressure. In contrast, RADAR’s run time checksum operations and FaR’s unstructured sparse index accesses both trigger repeated graph breaks under `torch.compile`, yielding overheads of +63–84% and +337–477% respectively.

Overall, RoR achieves the lowest latency and smallest storage footprint across all models and configurations. On Llama-2-7B, RoR runs  $1.7\times$  faster than RADAR and  $5.3\times$  faster than FaR, while incurring only +0.31% extra storage against +50% for RADAR and +3.04% for FaR. Combined with a theoretical FLOPs increase of <1%, these results confirm that RoR imposes negligible overhead in both compute and memory dimensions, with latency overhead ranging from +9.1% to +19.2% across all evaluated models.

#### G. Ablation Study: Effect of Outlier Threshold $\alpha$ (RQ6)

The threshold parameter  $\alpha$  dictates the aggressiveness of RoR’s outlier identification. Reducing  $\alpha$  incorporates more feature dimensions into the orthogonal rotation, thereby expanding the defensive coverage at the cost of marginally

TABLE III

INFERENCE LATENCY AND STORAGE OVERHEAD. EXTRA STORAGE IS RELATIVE TO THE BFLOAT16 MODEL WEIGHT FOOTPRINT; LATENCY OVERHEAD IS RELATIVE TO THE UNPROTECTED BASELINE.

Model	Method	Extra Storage	Latency (ms) $\downarrow$	Latency Overhead
OPT-125M	Baseline	—	46.71	—
	FaR	+2.10%	204.15	+336.9%
	RADAR	+50.0%	76.20	+63.1%
	RoR (Ours)	+0.23%	<b>52.28</b>	+11.9%
Qwen2.5-0.5B	Baseline	—	139.98	—
	FaR	+2.20%	707.12	+405.2%
	RADAR	+50.0%	238.37	+70.3%
	RoR (Ours)	+0.17%	<b>166.87</b>	+19.2%
LLaMA2-7B	Baseline	—	1052.24	—
	FaR	+3.04%	6075.90	+477.4%
	RADAR	+50.0%	1937.38	+84.1%
	RoR (Ours)	+0.31%	<b>1148.00</b>	+9.1%

TABLE IV

ABLATION ON THE OUTLIER THRESHOLD  $\alpha$ . *Count* DENOTES THE NUMBER OF ROTATED FEATURE DIMENSIONS (EFFICIENCY PROXY); *PPL@50* INDICATES THE PERPLEXITY AFTER ENDURING 50 TARGETED PBS BIT-FLIPS.

Config ( $\alpha$ )	Llama-3.2-1B		Llama-2-7B	
	Count	PPL@50	Count	PPL@50
Conservative ( $\alpha=9.0$ )	208	7,136	2,118	72,192
Standard ( $\alpha=6.0$ )	837	11,776	3,973	<b>26.3</b>
Aggressive ( $\alpha=3.0$ )	5,253	<b>158.0</b>	11,341	<b>23.9</b>

higher storage and computation for the auxiliary Compact WY factors. Table IV reports the number of rotated columns (serving as an efficiency overhead proxy) alongside the post-attack PPL after 50 PBS bit-flips across three  $\alpha$  configurations on Llama-3.2-1B and Llama-2-7B, directly quantifying the robustness–efficiency trade-off.

**Robustness–Efficiency Trade-off.** Reducing  $\alpha$  from 9.0 to 3.0 drastically expands the rotational coverage, increasing the protected column count by  $25\times$  on Llama-3.2-1B (208  $\rightarrow$  5,253) and  $5\times$  on Llama-2-7B (2,118  $\rightarrow$  11,341). The resulting robustness improvements, however, are substantial. On Llama-2-7B, transitioning to the standard setting ( $\alpha=6.0$ ) abruptly drops the post-attack PPL from a catastrophic 72,192 to 26.3, successfully neutralizing the SPoFs with only  $\approx 4k$  rotated dimensions (a minimal footprint). Conversely, Llama-3.2-1B requires the aggressive setting ( $\alpha=3.0$ ) to stabilize the model to a PPL of 158.0, incurring a proportionally higher overhead of  $\approx 5k$  dimensions.

**Architecture Sensitivity.** The distinct sensitivities to  $\alpha$  across evaluated models reveal fundamental differences in their internal activation distributions and structural vulnerabilities. Llama-2-7B achieves robust protection at  $\alpha=6.0$ , indicating that its activation outliers are extremely acute and heavily concentrated within a tiny fraction of feature channels. In contrast, the necessity of  $\alpha=3.0$  for Llama-3.2-1B—a phenomenon consistently observed in other highly optimized architectures such as Qwen2.5-7B—demonstrates that certain models exhibit a less extreme, but more spatially dispersed distribution of critical activation magnitudes. This broader dimensional vulnerability inherently requires wider orthogonal rotation coverage to sufficiently smooth these dispersed magnitudes and eliminate the latent SPoFs.

**Practical Recommendation.** The threshold  $\alpha$  serves as a principled, architecture-aware tunable parameter for practical deployments. Rather than strictly correlating with parameter scale, the optimal configuration is strictly governed by the intrinsic outlier distribution pattern of the target model. Architectures with highly concentrated outliers can operate at near-zero overhead using a standard threshold ( $\alpha=6.0$ ). Conversely, architectures characterized by a spatially dispersed vulnerability profile must adopt an aggressive setting ( $\alpha=3.0$ ) to guarantee sufficient defensive coverage against widespread latent faults. In all regimes, the number of dynamically rotated dimensions remains a minuscule fraction of the total hidden dimensions, confirming that RoR scales efficiently and adaptively across diverse LLM architectures.

## VI. DISCUSSION AND FUTURE WORK

While RoR provides a structurally lossless defense against bit-flip attacks, we identify three primary avenues for future system-level optimization and cross-domain extension.

### A. Overcoming Memory-Bound Bottlenecks

Although RoR introduces a mathematically negligible FLOP overhead ( $< 1\%$ ), empirical inference latency increases by 10%–20%. This discrepancy stems from the memory-bound nature of modern GPUs. The low-rank WY updates exhibit extremely low *arithmetic intensity*; execution time is dominated by repetitive DRAM read/write latencies for the Householder factors ( $\mathbf{V}$  and  $\mathbf{T}$ ) rather than actual computation. Future hardware–software co-design can eliminate this redundant memory traffic by developing custom, fused execution kernels (e.g., via Triton or CUDA) that persist these low-rank factors strictly within SRAM or registers.

### B. Scope Limitation: Normalization Layers

RoR currently secures dense linear projections, which constitute the vast majority of LLM parameters. However, the orthogonal rotation cannot be directly applied to normalization operations like RMSNorm. Mathematically, RMSNorm scales a normalized input  $\mathbf{x}$  by a learned parameter  $\gamma$  via element-wise multiplication ( $\odot$ ). Because an orthogonal matrix  $\mathbf{Q}$  does not commute with this operation—i.e.,  $\mathbf{Q}(\mathbf{x} \odot \gamma) \neq (\mathbf{Q}\mathbf{x}) \odot \gamma$ —applying  $\mathbf{Q}$  would improperly mix feature dimensions and destroy channel independence. Securing this minuscule parameter fraction without breaking its mathematical properties remains an open challenge.

### C. Limitations and Extension to Multimodal Architectures

While the mathematical formulation of RoR is structurally modality-agnostic, its practical extension to Multimodal LLMs (MLLMs) presents unique challenges due to fundamental distributional shifts. RoR relies on identifying static, persistent channel-wise outliers via offline calibration. However, recent empirical analyses reveal that multimodal tokens and their intermediate layer activations exhibit significantly higher statistical variance and entropy compared to purely textual tokens [44]. Consequently, visual outliers are highly dynamic

and input-dependent rather than being strictly confined to fixed hidden channels. This high-entropy distribution implies that an offline-calibrated, static rotation matrix may fail to intercept image-specific outlier spikes during runtime, or it may require a substantially larger number of target channels that severely degrades the efficiency of the low-rank WY representation. Therefore, successfully extending this lossless defense to multimodal architectures necessitates a paradigm shift from static offline rotation to dynamic, variance-aware orthogonal transformations that can adaptively secure localized spatial features.

## VII. RELATED WORK

Existing defenses against hardware-induced Bit-Flip Attacks (BFAs) were primarily tailored for conventional Deep Neural Networks (e.g., CNNs) and smaller-scale Transformers (e.g., ViTs). However, they face unique architectural and computational challenges when scaling to billion-parameter, autoregressive Large Language Models (LLMs). We classify these prior methodologies into two dominant paradigms: detection-based monitors and weight-robustness mechanisms.

1) *Detection-based Monitors*. Detection-based methods aim to intercept hardware faults during inference by introducing runtime monitors and redundancy checks. Monitor-centric approaches, such as NeuroPots [18], ModelShield [19], Weight-Sentry [45], Aegis [46], and anomaly detection schemes [47], rely on honey neurons, hash verification, range checks, or early-exit classifiers. Alternatively, software-based Error Correction Code (ECC) schemes [20], [21], [48], [49] integrate parity decoding directly into the computation path. To address the severe overhead of continuous verification, RADAR [17] serves as a pioneering baseline that embeds interleaved group checksums within the weight matrices. By computing lightweight addition-based checksums of the quantized weights, RADAR successfully detects parameter corruption with negligible latency on traditional CNNs architectures.

However, translating such layer-by-layer runtime verification to autoregressive LLMs presents structural challenges. LLM inference is inherently memory-bandwidth bound. Enforcing integrity verification on weight matrices for every generated token introduces strict synchronization barriers that can impede high-throughput token generation. Furthermore, the detection efficacy of these group-based checksums heavily depends on the grouping granularity. Sophisticated adversaries can systematically craft targeted, multi-bit attacks designed to bypass group-level parity checks, silently corrupting the LLM’s output.

2) *Weight-Robustness and Parameter Hardening*. Instead of monitoring for runtime errors, weight-robustness methods aim to inherently improve the fault tolerance of the model parameters. While methods like robust retraining (e.g., SAR [22] and WRecon [50]) are computationally prohibitive at the LLM scale, encoding-based defenses (e.g., DeepNcode [24], CodeNet [51], and RREC [25]) demand complex codeword recovery on the inference path. Consequently, post-training weight modification has emerged as a more practical alternative.

Notably, FaR (Forget-and-Rewire) [43] is a representative training-free hardening method. FaR structurally mitigates worst-case vulnerabilities by rewiring linear layers, redistributing the functional importance of critical neurons to less essential ones. While FaR reports minimal inference latency overheads on CNNs or ViTs, applying its sparse rewire operations to autoregressive LLMs incurs severe latency bottlenecks (e.g., up to 500% overhead in our evaluations) as unstructured memory accesses compound over sequential token generation steps. Furthermore, securing massive LLMs against aggressive targeted attacks requires applying higher hyperparameter configurations (e.g., larger rewiring ratios). This forced redistribution inherently distorts the pre-trained weight distribution, which inevitably degrades the model’s baseline accuracy and generative capabilities.

Unlike these prior paradigms, Rotated Robustness (RoR) achieves true lossless robustness. By applying matched orthogonal transformations to both the activation space and the weight matrices, RoR fundamentally neutralizes outlier-driven vulnerabilities while mathematically guaranteeing the perfect preservation of the model’s original generative accuracy. Furthermore, by formulating these rotations as hardware-friendly, dense low-rank matrix multiplications, RoR minimizes both inference latency and storage overhead, completely avoiding the synchronization barriers and unstructured sparsity inherent in prior defense schemes.

## VIII. CONCLUSION

This paper investigates the catastrophic vulnerability of Large Language Models (LLMs) to hardware-induced bit-flip attacks. We demonstrate that these sudden model collapses stem fundamentally from the spatial alignment between sensitive weight bits and extreme activation outliers. To neutralize this threat, we propose Rotated Robustness (RoR), a training-free defense utilizing orthogonal Householder transformations to geometrically smooth these outliers across all feature dimensions. By breaking this dangerous alignment, RoR mathematically guarantees true lossless robustness—preserving the model’s original accuracy and perplexity.

Extensive empirical evaluations confirm RoR’s superior reliability across diverse LLM families. Under black-box random fault injections, RoR effectively eliminates the risk of stochastic model collapse. Under gray-box scenarios involving targeted bit-search capabilities, RoR consistently sustains robust reasoning performance, maintaining near-lossless baseline accuracy where competing defenses suffer catastrophic failure. Against the most severe white-box Single Point Failure Attacks (SPFA) with full system visibility, RoR drastically increases the required number of targeted bit-flips, thereby pushing the attack complexity far beyond the physical limitations of Rowhammer. Furthermore, RoR achieves this state-of-the-art robustness with a negligible storage footprint and minimal inference latency, delivering a highly efficient, scalable, and reliable defense for real-world LLM deployments.

TABLE V  
COMPLETE PPL RESULTS UNDER GRAY-BOX PBS ATTACK ACROSS THREE MODEL ARCHITECTURES. RESULTS EXCEEDING  $10^{15}$  ARE MARKED WITH †.

#Flips	Llama-2-7B				Llama-3.2-1B				Qwen2.5-7B			
	Baseline	RoR	FaR	RADAR	Baseline	RoR	FaR	RADAR	Baseline	RoR	FaR	RADAR
0	5.03	5.03	8.00	5.03	9.06	9.19	10.12	9.06	5.41	5.41	6.56	5.41
1	5.66	5.19	12.38	5.03	20.12	9.19	13.81	9.06	—	—	—	—
2	7.28	5.16	13.19	5.03	27.88	9.31	19.75	9.06	$9.40 \times 10^2$	6.41	8.25	5.41
3	105.00	5.25	17.75	5.03	56.25	9.50	30.12	9.06	—	—	—	—
4	—	—	—	—	—	—	—	—	$7.62 \times 10^3$	43.25	7.09	5.41
5	$6.72 \times 10^3$	5.28	90.00	5.09	$1.70 \times 10^3$	9.81	60.00	9.06	—	—	—	—
6	—	—	—	—	—	—	—	—	$2.22 \times 10^{11}$	7.75	7.88	5.41
8	—	—	—	—	—	—	—	—	$5.42 \times 10^{13}$	12.94	7.28	5.41
10	$4.38 \times 10^4$	5.41	$2.90 \times 10^3$	5.12	$1.18 \times 10^4$	10.94	752.00	9.50	$3.54 \times 10^{14}$	11.25	11.44	5.41
12	—	—	—	—	—	—	—	—	$1.58 \times 10^{15}$	34.25	28.38	5.41
14	—	—	—	—	—	—	—	—	$9.15 \times 10^{15}†$	58.00	$8.10 \times 10^3$	5.41
16	—	—	—	—	—	—	—	—	$6.40 \times 10^{17}†$	82.00	$1.05 \times 10^5$	5.41
18	—	—	—	—	—	—	—	—	$1.95 \times 10^{11}$	119.50	$1.20 \times 10^6$	5.50
19	—	—	—	—	—	—	—	—	$4.84 \times 10^8$	237.00	$2.74 \times 10^7$	5.50
20	$5.99 \times 10^4$	5.56	$2.22 \times 10^5$	5.25	$2.11 \times 10^6$	13.56	$1.63 \times 10^5$	9.94	—	—	—	—
30	$4.35 \times 10^3$	6.53	$9.54 \times 10^7$	5.50	$3.70 \times 10^6$	25.75	$7.83 \times 10^6$	11.81	—	—	—	—
40	$9.88 \times 10^4$	10.94	$1.11 \times 10^{10}$	$2.62 \times 10^3$	$2.02 \times 10^8$	148.00	$4.35 \times 10^3$	13.56	—	—	—	—
50	$3.01 \times 10^4$	26.25	$8.16 \times 10^{10}$	$5.92 \times 10^3$	$7.44 \times 10^7$	$1.18 \times 10^4$	$5.73 \times 10^6$	15.88	—	—	—	—
60	$3.01 \times 10^4$	68.00	$2.39 \times 10^{12}$	$1.52 \times 10^4$	$1.39 \times 10^8$	$2.09 \times 10^5$	$1.98 \times 10^6$	22.75	—	—	—	—
70	$5.02 \times 10^5$	304.00	$1.64 \times 10^{12}$	$1.61 \times 10^4$	$2.79 \times 10^9$	$6.49 \times 10^6$	$3.11 \times 10^7$	19.12	—	—	—	—
80	$6.49 \times 10^6$	$2.46 \times 10^3$	$6.16 \times 10^{13}$	$8.64 \times 10^3$	$7.58 \times 10^9$	$1.49 \times 10^9$	$8.01 \times 10^8$	90.00	—	—	—	—
90	$1.39 \times 10^8$	$1.72 \times 10^4$	$7.48 \times 10^{14}$	$8.64 \times 10^3$	$2.64 \times 10^{10}$	$8.16 \times 10^{10}$	$8.59 \times 10^9$	131.00	—	—	—	—
100	$1.69 \times 10^9$	$1.27 \times 10^5$	$1.58 \times 10^{15}$	$8.64 \times 10^3$	$6.01 \times 10^{11}$	$2.07 \times 10^{10}$	$6.55 \times 10^4$	148.00	—	—	—	—

## APPENDIX A

### FULL PPL RESULTS UNDER GRAY-BOX PBS ATTACK

Table V provides the complete numerical Perplexity (PPL) degradation results corresponding to the visualization in Section V-C (Fig. 7). The results demonstrate the progressive collapse of baseline defenses under the gray-box Progressive Bit Search (PBS) attack across Llama-2-7B, Llama-3.2-1B, and Qwen2.5-7B architectures.

## REFERENCES

- [1] T. Brown, B. Mann, N. Ryder, M. Subbiah, J. D. Kaplan, P. Dhariwal, A. Neelakantan, P. Shyam, G. Sastry, A. Askell, S. Agarwal, A. Herbert-Voss, G. Krueger, T. Henighan, R. Child, A. Ramesh, D. Ziegler, J. Wu, C. Winter, C. Hesse, M. Chen, E. Sigler, M. Litwin, S. Gray, B. Chess, J. Clark, C. Berner, S. McCandlish, A. Radford, I. Sutskever, and D. Amodei, “Language models are few-shot learners,” in *Advances in Neural Information Processing Systems*, vol. 33. Curran Associates, Inc., 2020, pp. 1877–1901.
- [2] H. Touvron, L. Martin, K. Stone, P. Albert, A. Almahairi, Y. Babaei, N. Bashlykov, S. Batra, P. Bhargava, S. Bhosale *et al.*, “Llama 2: Open foundation and fine-tuned chat models,” 2023.
- [3] A. Grattafiori, A. Dubey, A. Jauhri, A. Pandey, A. Kadian, A. Al-Dahle, A. Letman, A. Mathur, A. Schelten, A. Vaughan, A. Yang, A. Fan *et al.*, “The llama 3 herd of models,” 2024.
- [4] J. Bai, S. Bai, Y. Chu, Z. Cui, K. Dang, X. Deng, Y. Fan, W. Ge, Y. Han, F. Huang *et al.*, “Qwen technical report,” 2023.
- [5] OpenAI, J. Achiam, S. Adler, S. Agarwal, L. Ahmad, I. Akkaya, F. L. Aleman, D. Almeida, J. Altschmidt, S. Altman, S. Anadkat *et al.*, “Gpt-4 technical report,” 2024.
- [6] J. Wei, X. Wang, D. Schuurmans, M. Bosma, b. ichter, F. Xia, E. Chi, Q. V. Le, and D. Zhou, “Chain-of-thought prompting elicits reasoning in large language models,” in *Advances in Neural Information Processing Systems*, vol. 35. Curran Associates, Inc., 2022, pp. 24 824–24 837.
- [7] D. Narayanan, M. Shoenybi, J. Casper, P. LeGresley, M. Patwary, V. Korthikanti, D. Vainbrand, P. Kashinkunti, J. Bernauer, B. Catanzaro, A. Phanishayee, and M. Zaharia, “Efficient large-scale language model training on gpu clusters using megatron-lm,” in *Proceedings of the International Conference for High Performance Computing, Networking, Storage and Analysis (SC)*, ser. SC ’21. New York, NY, USA: Association for Computing Machinery, 2021.
- [8] Z. Liu, C. Zhao, F. Iandola, C. Lai, Y. Tian, I. Fedorov, Y. Xiong, E. Chang, Y. Shi, R. Krishnamoorthi, L. Lai, and V. Chandra, “MobileLLM: Optimizing sub-billion parameter language models for on-device use cases,” in *Forty-first International Conference on Machine Learning*, 2024.
- [9] J. S. Park, J. O’Brien, C. J. Cai, M. R. Morris, P. Liang, and M. S. Bernstein, “Generative agents: Interactive simulacra of human behavior,” in *Proceedings of the Annual ACM Symposium on User Interface Software and Technology (UIST)*, ser. UIST ’23. New York, NY, USA: Association for Computing Machinery, 2023.
- [10] S. Wu, O. Irsoy, S. Lu, V. Dabravolski, M. Dredze, S. Gehrmann, P. Kambadur, D. Rosenberg, and G. Mann, “Bloomberggpt: A large language model for finance,” 2023.
- [11] Y. Kim, R. Daly, J. Kim, C. Fallin, J. H. Lee, D. Lee, C. Wilkerson, K. Lai, and O. Mutlu, “Flipping bits in memory without accessing them: an experimental study of dram disturbance errors,” in *Proceeding of the 41st Annual International Symposium on Computer Architecture*, ser. ISCA ’14. IEEE Press, 2014, p. 361–372.
- [12] Z. Zhang, W. He, Y. Cheng, W. Wang, Y. Gao, M. Wang, K. Li, S. Nepal, and Y. Xiang, “Bitmine: An end-to-end tool for detecting rowhammer vulnerability,” *IEEE Transactions on Information Forensics and Security*, vol. 16, pp. 5167–5181, 2021.
- [13] A. S. Rakin, Z. He, and D. Fan, “Bit-flip attack: Crushing neural network with progressive bit search,” in *Proceedings of the IEEE/CVF International Conference on Computer Vision (ICCV)*, 2019.
- [14] S. Hong, P. Frigo, Y. Kaya, C. Giuffrida, and T. Dumitras, “Terminal brain damage: Exposing the graceless degradation in deep neural networks under hardware fault attacks,” in *28th USENIX Security Symposium (USENIX Security 19)*. Santa Clara, CA: USENIX Association, Aug. 2019, pp. 497–514.
- [15] X. Li, Y. Meng, J. Chen, L. Luo, and Q. Zeng, “Rowhammer-based trojan injection: One bit flip is sufficient for backdooring dnns,” in *34th USENIX Security Symposium (USENIX Security 25)*. Seattle, WA, USA: USENIX Association, 2025, pp. 6319–6337.
- [16] S. Das, S. Bhattacharya, S. Kundu, S. Kundu, A. Menon, A. Raha, and K. Basu, “Attentionbreaker: Adaptive evolutionary optimization for unmasking vulnerabilities in LLMs through bit-flip attacks,” *Transactions on Machine Learning Research*, 2025.
- [17] J. Li, A. S. Rakin, Z. He, D. Fan, and C. Chakrabarti, “Radar: Runtime adversarial weight attack detection and accuracy recovery,” in *2021 Design, Automation & Test in Europe Conference & Exhibition (DATE)*, 2021, pp. 790–795.
- [18] Q. Liu, J. Yin, W. Wen, C. Yang, and S. Sha, “NeuroPots: Realtime proactive defense against Bit-Flip attacks in neural networks,” in *32nd USENIX Security Symposium (USENIX Security 23)*. Anaheim, CA: USENIX Association, Aug. 2023, pp. 6347–6364.
- [19] Y. Guo, L. Liu, Y. Cheng, Y. Zhang, and J. Yang, “Modelshield: A generic and portable framework extension for defending bit-flip based

- adversarial weight attacks,” in *2021 IEEE 39th International Conference on Computer Design (ICCD)*, 2021, pp. 559–562.
- [20] H. Liu, V. Singh, M. Filipiuk, and S. K. S. Hari, “Alberta: Algorithm-based error resilience in transformer architectures,” *IEEE Open Journal of the Computer Society*, vol. 6, pp. 85–96, 2025.
- [21] S. T. Ahmed, S. Hemaram, and M. B. Tahoori, “Nn-ecc: Embedding error correction codes in neural network weight memories using multi-task learning,” in *2024 IEEE 42nd VLSI Test Symposium (VTS)*, 2024, pp. 1–7.
- [22] C. Zhou, J. Du, M. Yan, H. Yue, X. Wei, and J. T. Zhou, “Sar: Sharpness-aware minimization for enhancing dnn’s robustness against bit-flip errors,” *Journal of Systems Architecture*, vol. 156, p. 103284, 2024.
- [23] J. Li, A. S. Rakin, Y. Xiong, L. Chang, Z. He, D. Fan, and C. Chakrabarti, “Defending bit-flip attack through dnn weight reconstruction,” in *2020 57th ACM/IEEE Design Automation Conference (DAC)*, 2020, pp. 1–6.
- [24] P. Velčický, J. Breier, M. Kovačević, and X. Hou, “Deepncode: Encoding-based protection against bit-flip attacks on neural networks,” 2024.
- [25] L. Liu, Y. Guo, Y. Cheng, Y. Zhang, and J. Yang, “Generating robust dnn with resistance to bit-flip based adversarial weight attack,” *IEEE Transactions on Computers*, vol. 72, no. 2, pp. 401–413, 2023.
- [26] T. Dettmers, M. Lewis, Y. Belkada, and L. Zettlemoyer, “Gpt3.int8(): 8-bit matrix multiplication for transformers at scale,” in *Advances in Neural Information Processing Systems*, vol. 35. Curran Associates, Inc., 2022, pp. 30 318–30 332.
- [27] G. Xiao, J. Lin, M. Seznec, H. Wu, J. Demouth, and S. Han, “SmoothQuant: Accurate and efficient post-training quantization for large language models,” in *Proceedings of the 40th International Conference on Machine Learning*, ser. Proceedings of Machine Learning Research, vol. 202. PMLR, 2023, pp. 38 087–38 099.
- [28] A. S. Householder, “Unitary triangularization of a nonsymmetric matrix,” *J. ACM*, vol. 5, no. 4, p. 339–342, Oct. 1958.
- [29] A. Vaswani, N. Shazeer, N. Parmar, J. Uszkoreit, L. Jones, A. N. Gomez, L. u. Kaiser, and I. Polosukhin, “Attention is all you need,” in *Advances in Neural Information Processing Systems*, vol. 30. Curran Associates, Inc., 2017.
- [30] E. Frantar, S. Ashkboos, T. Hoefler, and D. Alistarh, “OPTQ: Accurate quantization for generative pre-trained transformers,” in *The Eleventh International Conference on Learning Representations*, 2023.
- [31] R. Baumann, “Radiation-induced soft errors in advanced semiconductor technologies,” *IEEE Transactions on Device and Materials Reliability*, vol. 5, no. 3, pp. 305–316, 2005.
- [32] K. K. Chang, A. G. Yağlıkçı, S. Ghose, A. Agrawal, N. Chatterjee, A. Kashyap, D. Lee, M. O’Connor, H. Hassan, and O. Mutlu, “Understanding reduced-voltage operation in modern dram devices: Experimental characterization, analysis, and mechanisms,” *Proc. ACM Meas. Anal. Comput. Syst.*, vol. 1, no. 1, Jun. 2017.
- [33] N. Carlini, A. Athalye, N. Papernot, W. Brendel, J. Rauber, D. Tsipras, I. Goodfellow, A. Madry, and A. Kurakin, “On evaluating adversarial robustness,” 2019.
- [34] J. Guo, C. Chakrabarti, and D. Fan, “Sbfa: Single sneaky bit flip attack to break large language models,” 2025.
- [35] F. Yao, A. S. Rakin, and D. Fan, “DeepHammer: Depleting the intelligence of deep neural networks through targeted chain of bit flips,” in *29th USENIX Security Symposium (USENIX Security 20)*. USENIX Association, Aug. 2020, pp. 1463–1480.
- [36] R. Schreiber and C. Van Loan, “A storage-efficient \$wy\$ representation for products of householder transformations,” *SIAM Journal on Scientific and Statistical Computing*, vol. 10, no. 1, pp. 53–57, 1989. [Online]. Available: <https://doi.org/10.1137/0910005>
- [37] S. Zhang, S. Roller, N. Goyal, M. Artetxe, M. Chen, S. Chen, C. Dewan, M. Diab, X. Li, X. V. Lin, T. Mihaylov, M. Ott, S. Shleifer, K. Shuster, D. Simig, P. S. Koura, A. Sridhar, T. Wang, and L. Zettlemoyer, “Opt: Open pre-trained transformer language models,” 2022.
- [38] A. Yang, B. Yang, B. Hui, B. Zheng, B. Yu, C. Zhou, C. Li *et al.*, “Qwen2 technical report,” 2024.
- [39] S. Merity, C. Xiong, J. Bradbury, and R. Socher, “Pointer sentinel mixture models,” 2016.
- [40] R. Zellers, A. Holtzman, Y. Bisk, A. Farhadi, and Y. Choi, “HellaSwag: Can a machine really finish your sentence?” in *Proceedings of the 57th Annual Meeting of the Association for Computational Linguistics*. Florence, Italy: Association for Computational Linguistics, Jul. 2019, pp. 4791–4800.
- [41] D. Hendrycks, C. Burns, S. Basart, A. Zou, M. Mazeika, D. Song, and J. Steinhardt, “Measuring massive multitask language understanding,” in *International Conference on Learning Representations*, 2021.
- [42] Y. Bisk, R. Zellers, R. Le bras, J. Gao, and Y. Choi, “Piqa: Reasoning about physical commonsense in natural language,” *Proceedings of the AAAI Conference on Artificial Intelligence*, vol. 34, no. 05, pp. 7432–7439, 2020.
- [43] N. Nazari, H. M. Makrani, C. Fang, H. Sayadi, S. Rafatirad, K. N. Khasawneh, and H. Homayoun, “Forget and rewire: Enhancing the resilience of transformer-based models against Bit-Flip attacks,” in *33rd USENIX Security Symposium (USENIX Security 24)*. Philadelphia, PA: USENIX Association, Aug. 2024, pp. 1349–1366.
- [44] S. Bhatnagar, A. Xu, K.-H. Tan, and N. Ahuja, “Luq: Layerwise ultra-low bit quantization for multimodal large language models,” 2025.
- [45] M. Abumandour, S. Ramischetty, G. Venkataramani, and A. Alameldeen, “Weightsentry: Real-time bit-flip protection for deep neural networks on gpus,” in *Proceedings of the 14th International Workshop on Hardware and Architectural Support for Security and Privacy*, ser. HASP ’25. New York, NY, USA: Association for Computing Machinery, 2025, p. 91–99.
- [46] J. Wang, Z. Zhang, M. Wang, H. Qiu, T. Zhang, Q. Li, Z. Li, T. Wei, and C. Zhang, “Aegis: Mitigating targeted bit-flip attacks against deep neural networks,” in *32nd USENIX Security Symposium (USENIX Security 23)*. Anaheim, CA: USENIX Association, Aug. 2023, pp. 2329–2346.
- [47] K. Wen, X. Wang, J. Zhao, F. Xu, and Y. Wang, “Anomaly-driven defense: Mitigating bit-flip attacks in deep neural networks via runtime parameter clipping,” in *Advanced Intelligent Computing Technology and Applications*. Singapore: Springer Nature Singapore, 2025, pp. 370–382.
- [48] H. Guan, L. Ning, Z. Lin, X. Shen, H. Zhou, and S.-H. Lim, “In-place zero-space memory protection for cnn,” in *Advances in Neural Information Processing Systems*, vol. 32. Curran Associates, Inc., 2019.
- [49] S.-S. Lee and J.-S. Yang, “Value-aware parity insertion ecc for fault-tolerant deep neural network,” in *2022 Design, Automation & Test in Europe Conference & Exhibition (DATE)*, 2022, pp. 724–729.
- [50] Z. He, A. S. Rakin, J. Li, C. Chakrabarti, and D. Fan, “Defending and harnessing the bit-flip based adversarial weight attack,” in *Proceedings of the IEEE/CVF Conference on Computer Vision and Pattern Recognition (CVPR)*, 2020.
- [51] S. Dutta, Z. Bai, T. M. Low, and P. Grover, “Codenet: Training large scale neural networks in presence of soft-errors,” 2019.